

# Non-Equilibrium Oscillations Arising in Thermally Induced Convective Systems through Homodyne Dynamic Light Scattering

José López-Molina,<sup>1</sup> Arturo Moncho-Jordá,<sup>1,2,\*</sup> and María Tirado-Miranda<sup>1,†</sup>

<sup>1</sup>*Department of Applied Physics, Universidad de Granada, Campus Fuentenueva S/N, 18071 Granada, Spain.*

<sup>2</sup>*Institute Carlos I for Theoretical and Computational Physics, Universidad de Granada, Campus Fuentenueva S/N, 18071 Granada, Spain.*

(Dated: April 4, 2024)

We use Homodyne Dynamic Light Scattering (HDLS) with a dual-laser beam setup to investigate the drift velocities of colloidal particles immersed in a solvent exposed to thermally-induced convection. Our investigation reveals the appearance of oscillations of a well-defined frequency in the intensity autocorrelation function, which are linked to the particle drift velocities. In addition to this non-equilibrium oscillations, we report an enhanced decay of the intensity correlation function attributable to the loss of correlation as particles depart from the scattering volume due to prevailing convective flow. A pivotal discovery of our research is the identification of a specific temperature gradient threshold, beyond which pronounced velocity fluctuations ensue as a consequence of the establishment of a non-stationary flow within the measurement cell. The experimental results, obtained for different colloidal systems, are corroborated by a theoretical model and thoroughly validated with fluid dynamics simulations and Brownian dynamics simulations, yielding excellent agreement with the experimental data, and providing a robust and complete explanation of the observed phenomena. This study presents an insight in the field of non-equilibrium particle dynamics, offering a reliable method to study complex behaviors in convective systems through advanced HDLS techniques and multidisciplinary simulations.

Convection-diffusion phenomena are non-equilibrium processes inherent to a multitude of physical, chemical, and biological phenomena. Heat transport [1], transportation mechanisms in the brain's interstitium [2], pattern generation [3], or particle segregation processes [3] exemplify the universality of these phenomena. To fully comprehend these behaviors, it is essential to reexamine and adapt techniques traditionally used for systems in equilibrium focusing on understanding how these non-equilibrium processes influence measurements.

In the context of non-equilibrium dynamics, we are particularly interested in techniques capable of measuring system dynamics, as they offer the most valuable insights. Recent studies have made significant advancements in this domain. For instance, expanding the application of Dynamic Light Scattering (DLS) to different cases like acousto-responsive microgels under ultrasonic influence [4], flow-induced current planes [5], and 3D imaging of heterogeneous diffusion and flow patterns [6]. Other similar techniques like X-ray Photon Correlation Spectroscopy (XPCS) have been enhanced to observe ballistic dynamics under magnetic fields [7], measure direction dependent diffusion of magnetic rods [8], inside living cells without harming them [9] or in colloidal palladium [10].

Light scattering techniques, particularly Homodyne Dynamic Light Scattering (HDLS), emerge as powerful tools for measuring under these non-equilibrium conditions. In such experiments, oscillatory behaviors have been reported [11–13], sparking considerable debate over their physical interpretation. This ambiguity extends to the anomalous decay of temporal intensity correlation in convective conditions, a phenomenon attributed to various causes [14–21]. Our work endeavors to provide a comprehensive explanation for these two phenomena by integrating theoretical analysis, experimental measurements, Brownian dynamics simulations (BD),

and fluid dynamic simulations. An advanced HDLS methodology is explored for quantifying the drift velocities of particles immersed in fluids subjected to induced thermal convection. This approach innovates by employing a two-beam setup, traditionally used in 3D-DLS for cross-correlation measurements, and adapting it for autocorrelation analysis.

For a single beam device, the field autocorrelation function of a monodisperse colloidal system of spherical colloids with diffusion coefficient  $D$  and drift velocity  $\mathbf{v}$  is given by [11, 13, 20, 22]

$$g^{(1)}(\mathbf{q}, \tau) = e^{i\mathbf{q}\cdot\mathbf{v}} e^{-Dq^2\tau}, \quad (1)$$

where  $\mathbf{q}$  is the scattering vector of the monochromatic laser beam. With the traditional one-beam HDLS it is only possible to measure the intensity correlation function, given by  $g^{(2)}(\mathbf{q}, \tau) = 1 + |g^{(1)}(\mathbf{q}, \tau)|^2 = 1 + e^{-2Dq^2\tau}$  [22–25]. As observed,  $\mathbf{v}$  does not have any effect on  $g^{(2)}$ , so the single-beam arrangement is not able to detect convective effects.

This situation changes for the case of a two-beam setup with scattering vectors  $\mathbf{q}_1$  and  $\mathbf{q}_2$ , respectively. Using that photons scattered by different beams are not intercorrelated, the intensity autocorrelation function is generalized to [26–29]

$$g^{(2)}(\mathbf{q}_1, \mathbf{q}_2, \tau) - 1 = |g^{(1)}(\mathbf{q}_1, \tau) + g^{(1)}(\mathbf{q}_2, \tau)|^2. \quad (2)$$

Extending the traditional single-beam autocorrelation function, modified for drift velocity ( $\mathbf{v}$ ), into our two-beams scenario, we find that

$$g^{(2)}(\mathbf{q}_1, \mathbf{q}_2, \tau) - 1 = e^{-2D\bar{q}^2\tau} [(1 - C) + C \cos(\Delta\mathbf{q} \cdot \mathbf{v}\tau)], \quad (3)$$

where  $\bar{q} = |\mathbf{q}_1 + \mathbf{q}_2|/2$  represents the modulus of the mean of both dispersion vectors,  $\Delta\mathbf{q} = \mathbf{q}_1 - \mathbf{q}_2$  is the scattering vectors' difference, and  $0 \leq C \leq 1$  represents the relative intensity of

each beam. Crucially, this model reveals an oscillatory component, with a characteristic frequency given by  $\omega = \Delta\mathbf{q} \cdot \mathbf{v}$ .

In the study of thermal convection, oscillations are not the sole non-equilibrium anomaly observed. Another significant finding is the discrepancy in diffusion coefficients when a drift velocity field is applied. The coefficient derived from the experimental decay of  $g^{(2)}(\tau)$  consistently exceeds the value predicted by the Stokes-Einstein equation,  $D_{st} = k_B T / (6\pi\eta a)$  (where  $k_B$  is the Boltzmann constant,  $T$  the absolute temperature,  $\eta$  is the solvent viscosity and  $a$  denotes the radius of the colloidal particles). This phenomenon has been previously reported in the literature as compressed exponential relaxations [19], attributed to an enhancement of the diffusion coefficient due to reduced friction caused by the convective flow [20] or discussed as superdiffusion [21]. The rapid decay of  $g^{(2)}(\tau)$  is linked to particles escaping the measurement volume due to convective velocity, resulting in a loss of correlation.

A proposed correction involves an exponential term dependent on velocity and time squared, based on a Gaussian laser beam intensity profile. However, this approach failed to accurately measure the diffusion coefficient for low drift velocities in our experiments [17, 30–33]. We reconsidered the laser beam profile's impact, focusing on the scattering volume defined by the intersection of laser beams and the detector's pinhole projection. This led us to treat the beam's intensity as uniform within the scattering region and 0 outside it.

The amplitude of the scattered electric field is thus considered constant across the beam thickness  $h$  ( $P(z) = E_0$  for  $-\frac{h}{2} < z < \frac{h}{2}$ ). This revised model introduces a new factor into the correlation function,  $\langle P(z(0))P(z(t)) \rangle g^{(1)}(\mathbf{q}, \tau)$ , where  $g^{(1)}(\mathbf{q}, \tau)$  is given by Eq. (1) and  $z(t) = vt + z_0$ , accounting for the observed diffusion coefficient increase by considering the velocity,  $v$ , effect and  $h$ . The modified field correlation function for a single-beam device is expressed as:

$$g^{(1)}(\mathbf{q}, \tau) = e^{i\mathbf{q} \cdot \mathbf{v}} e^{-Dq^2\tau} \left(1 - \frac{v\tau}{h}\right) \quad \tau \leq h/v, \quad (4)$$

and  $g^{(1)}(\mathbf{q}, \tau) = 0$  if  $\tau > h/v$ . The term  $1 - \frac{v\tau}{h}$  embodies the rate at which particles drift out of the scattering volume.

Combining Eqs. (2) and (4), a new expression arises that gathers both the oscillatory behavior and the faster loss of correlation for the two-beams arrangement:

$$g^{(2)}(\mathbf{q}_1, \mathbf{q}_2, \tau) - 1 = e^{-2D\bar{q}^2\tau} [(1 - C) + C \cos(\Delta\mathbf{q} \cdot \mathbf{v}\tau)] \left(1 - \frac{v\tau}{h}\right)^2 \quad (5)$$

for  $\tau < h/v$  and  $g^{(2)}(\mathbf{q}_1, \mathbf{q}_2, \tau) - 1 = 0$  for  $\tau > h/v$ .

In our experiments, we investigated oscillatory behaviors under convective flow using a 3D-DLS system from LS-Instruments. This system divides an incoming laser beam into two, each aligned with its respective detector at the same scattering angles,  $\theta$ , slightly shifted above and below the scattering plane. This ensures each detector-beam pair aligns along the same scattering vector. Our approach involved deactivating one detector, enabling the sole active detector to capture

signals from both beams, resulting in two distinct scattering vectors. We used monodisperse polystyrene spheres, with radius  $a = 406 \pm 10$  nm, from microparticles GmbH, Berlin, Germany, for consistency in our experiments. Measurements took place in a cylindrical glass cell by LS-Instruments, 0.8 cm in diameter and 7.5 cm height, with the sample filling up to 4 cm. Only the lower 1 cm portion of the cell was immersed in a temperature-controlled bath, with the upper part in contact with metal. Measurements were focused at the center of the cell, 0.5 cm from the bottom, where the beams of the dual-laser setup intersected. In all measurements the room temperature was  $T_{\text{Room}} = 23^\circ\text{C}$ .

Fig. 1(a) presents a comparison between single and dual-beam laser measurements with a bath temperature  $T = 38^\circ\text{C}$ . In the single-beam setup, the correlation function shows no oscillatory behavior, indicating that convective flow alone does not result in oscillations. In contrast, the dual-beam setup reveals clear oscillations of a well-defined frequency, confirming that the simultaneous use of two lasers is essential for observing this behavior in this system.

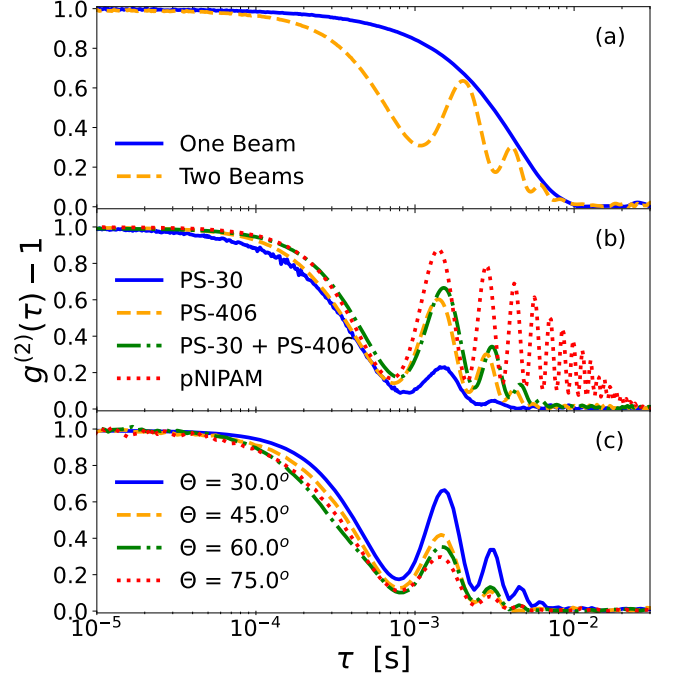


FIG. 1. Intensity autocorrelation functions,  $g^{(2)}(\tau) - 1$ , as a function of  $\tau$  obtained via 3D-DLS setup. Plot (a) shows the effect of the number of beams for a bath temperature  $T_{\text{Bath}} = 38^\circ\text{C}$  and measurement scattering angle  $\theta = 30^\circ$ . Plot (b) depicts the oscillatory effect for different kind of colloidal particles and sizes, for  $T_{\text{Bath}} = 40^\circ\text{C}$  and  $\theta = 30^\circ$ . Panel (c) shows that the oscillation frequency does not depend on  $\theta$ , for  $T_{\text{Bath}} = 40^\circ\text{C}$ . In all cases the room temperature was  $T_{\text{Room}} = 23^\circ\text{C}$ .

The oscillatory phenomenon observed in our experiments is not a particular result tied to specific particle types; rather, it is a universal behavior evident across a range of systems, including  $a = 406$  nm and 30 nm radius monodisperse polystyrene

particles, a mixture of these, and significantly larger pNIPAM microgels, as illustrated in Fig. 1(b). Particularly notable is the pronounced oscillation in the microgel system, likely attributable to its larger size, and showing that this is not a marginal effect but a dominant one, especially in larger particles. Contrary to the dependence on particle light absorption suggested in previous studies [11, 13, 15, 18], our findings indicate that light absorption is not a prerequisite of the system to exhibit oscillations. This underscores that thermal gradients inducing convection can be externally imposed and measured, regardless of particle composition. We observed this phenomenon in both monodisperse and bidisperse systems, indicating that all particles, regardless of size, move at a common velocity imposed by the convective flow of the solvent and challenging the assertion that bidispersity is necessary for oscillation occurrence [11].

Looking at the size-dependence of these oscillations, as particle size diminishes, the amplitude of the oscillations become less pronounced. This relationship is quantitatively explained by considering the condition derived from Eq. (5),  $\Delta\mathbf{q} \cdot \mathbf{v} / (2\pi) > D\bar{q}^2$ . It indicates that  $g^{(2)}(\tau)$  decays faster for particles with a larger diffusion coefficient (i.e., particles of smaller size), thus smoothing out the oscillations.

The influence of the detection angle on the autocorrelation function is illustrated in Fig 1(c), for a system comprised by polystyrene particles of radius  $a = 406$  nm. As observed, the oscillation amplitude decreases when increasing  $\theta$ , but the frequency becomes totally unaffected by changes in  $\theta$ . To elucidate both effects, we calculate  $\Delta\mathbf{q} = \mathbf{q}_1 - \mathbf{q}_2$ , where  $\mathbf{q}$  is the scattering vector defined by  $\mathbf{q} = \mathbf{k}_i - \mathbf{k}_f$  and its modulus is  $q = \frac{4\pi n}{\lambda} \sin\left(\frac{\theta}{2}\right)$ . Our configuration results in  $\Delta\mathbf{q} = (2\pi/\lambda)(0, 0, 2\sin(\phi))$ , where  $\phi = 0.052$  rad, indicating that  $\Delta\mathbf{q}$  only has a  $z$ -component, perpendicular to the scattering plane (i.e.  $z$  corresponds to the vertical direction). This results in the detection angle  $\theta$  not affecting  $\Delta\mathbf{q}$ . The constant frequency of oscillations across various detection angles confirms that we are accurately capturing a vertical velocity component,  $v_z$ , parallel to  $\Delta\mathbf{q}$ . This invariance in frequency with the detection angle aligns with our theoretical model, which posits that the frequency depends solely on  $\Delta\mathbf{q} \cdot \mathbf{v}$ . On the other hand, the decrease of the oscillatory amplitude with  $\theta$  is explained making use of the condition  $\Delta\mathbf{q} \cdot \mathbf{v} / (2\pi) > D\bar{q}^2$ . Indeed, increasing the measurement angle increases  $q$ , reducing observable oscillations. Therefore, to detect small drift velocities, low angles are preferable.

In Fig. 2(a) the experimental correlation functions for increasing the temperature gradient are depicted as symbols. For small  $\Delta T$  (when bath temperature is close to ambient temperature), the data show no oscillations in the correlation functions. This observation indicates that the convective currents are indeed driven by the thermal gradient. As  $\Delta T$  is increased, we observe the emergence of oscillations in the correlation functions, which shift towards the left. This shift signifies an increase in the vertical velocity of the particles,  $v_z$  (we remark that our two-beam setup can only detect the  $z$ -component of

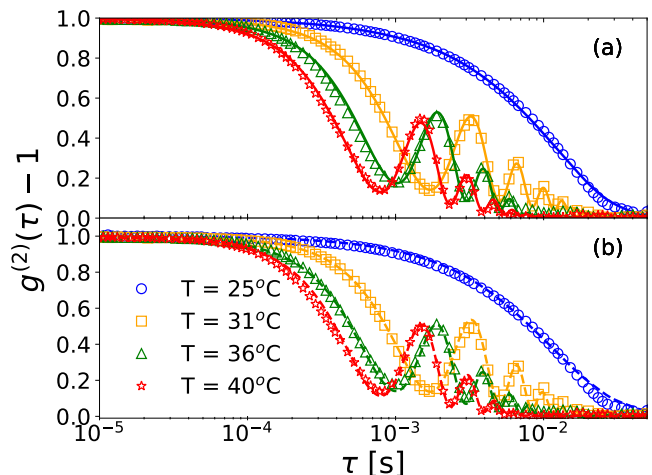


FIG. 2.  $g^{(2)}(\tau) - 1$  as a function of  $\tau$  for particles with a radius of  $a = 406$  nm, illuminated by two beams at different bath temperatures. Symbols represent the experimental measurements obtained via the 3D-DLS device. In plot (a), solid lines depict fits of the experimental data to the theoretical model (Eq. (5)). In plot (b), dashed lines represent correlation functions derived from BD simulations at velocities determined by the respective fits. In both panels  $\theta = 40^\circ$ , and the room temperature was  $T_{\text{Room}} = 23^\circ\text{C}$ .

the actual drift velocity).

$T$ [ $^\circ\text{C}$ ]	$D_{\text{st}}$ [ $\mu\text{m}^2/\text{s}$ ]	$D_{\text{fit}}$ [ $\mu\text{m}^2/\text{s}$ ]	$v_z$ [mm/s]	$C$
25	0.596	0.56	0.07	0.41
31	0.693	0.71	1.36	0.40
36	0.780	0.86	2.30	0.36
40	0.901	0.97	2.95	0.39

TABLE I. Values of  $D_{\text{fit}}$ ,  $v_z$  and  $C$  obtained by fitting the experimental data from Fig. (2) using Eq. (5) for different bath temperatures. The corresponding Stokes-Einstein diffusion coefficients,  $D_{\text{st}}$ , are also included for comparison.

The experimental results are compared with theoretical predictions as outlined by Eq.(5), depicted by solid lines in Fig.2(a). Data for the fitted diffusion coefficient ( $D_{\text{fit}}$ ), particle velocity ( $v_z$ ), and constant  $C$ , with the beam thickness set at  $h = 30\mu\text{m}$ , is presented in Table I. This table further lists expected Stokes-Einstein diffusion coefficients,  $D_{\text{st}}$ , calculated for different temperatures. As observed, Eq. (5) excellently captures the experimental data in all cases. The fitted  $D_{\text{fit}}$  values closely match the expected  $D_{\text{st}}$ , with discrepancies ranging from 5% to 8%. Crucially, neglecting the correction for particle exit from the dispersion volume (see Eq. 3) leads to  $D_{\text{fit}}$  values inaccurately increasing with temperature  $T$ , deviating from  $D_{\text{st}}$  values and significantly elevating the error over 100% at high drift velocities. The velocities obtained align with typical values for such measurement cells [14]. The parameter  $C$  was observed to stay consistently around 0.4, indicating the reliability of the theoretical framework. However, it was not possible to reproduce velocity measurements at temperatures above  $40^\circ\text{C}$ , which will be discussed later.

To further validate the proposed explanations, we conducted Brownian dynamics (BD) simulations on an ideal system, in which particles possessed the expected diffusion coefficient,  $D_{st}$ . The simulation employed a time step of  $10^{-5}$  s during a total time of 10 s and was set in a simulation cubic box with side  $h = 30 \mu\text{m}$ . A vertical upward flow was imposed along the  $z$ -axis representing the fluid velocity due to thermal convection. The associated values of  $v_z$  were extracted from our fits presented in Table I. Periodic boundary conditions were applied on the  $x$  and  $y$  directions. Particle motion combined random Brownian movement with a constant velocity component in the  $z$ -coordinate. When a particle exits the simulation box through the top, another one is randomly introduced at the bottom, maintaining constant the number of particles. The total scattered electric field of the system at each time step is calculated using  $E_s(t) = \sum_{i=1}^N [C \exp(i\mathbf{q}_1 \cdot \mathbf{r}_i(t)) + (1 - C) \exp(i\mathbf{q}_2 \cdot \mathbf{r}_i(t))]$ , where  $N = 100$  is the number of particles. The correlation function of  $E_s(t)$  was then determined and normalized. To account for our particular experimental setup,  $C = 0.4$  is used in the calculation of the autocorrelation function.

Fig. 2(b) presents the simulated correlation functions alongside the experimental data, showing a remarkable agreement with the experiments, thus confirming that our simulation accurately captures the loss of correlation arising when particles escape from the scattering volume due to the convective flow. The consistency between oscillation frequency,  $\omega = \Delta q v_z$ , obtained in the experiments and BD simulations shows that the velocity subtracted in our fits corresponds to the system's vertical drift velocity.

Building on the quantitative measurements of convective currents through our HDLS method, we now delve deeper into the convective phenomenon from a fluid dynamics perspective. Using the Nonisothermal Flow interface in COMSOL, free convection was modeled in water. This approach took into account both momentum and energy balances, offering insights into heat transfer through convection and conduction within the setup. Both the cell and water were initialized at  $T_{\text{Room}} = 23^\circ\text{C}$ . The cylindrical glass cell's base was positioned in a temperature bath that heated only its bottom-most 1 cm. Thus, this section of the external surface of the cell maintained a constant temperature, mirroring the bath's temperature. Above this heated segment, the cell's side walls, which were not submerged in the bath, were in direct contact with a metal component maintained at a steady room temperature, leading to a constant lateral temperature boundary for the cell. Internally, the boundary between the water and glass adhered to a no slip condition. The open surface of water, subject to ambient conditions, was characterized by a slip condition.

This model is used to explore the system response over time to a temperature difference between the bath and the room of  $\Delta T_{\text{BR}} = T_{\text{Bath}} - T_{\text{Room}} = 10^\circ\text{C}$ , at which oscillatory behavior in the correlation function was observed in our experiments. For this condition, the fluid dynamics simulation revealed that both the velocity and temperature profiles within the cell eventually reach a steady state. The stationary velocity profile

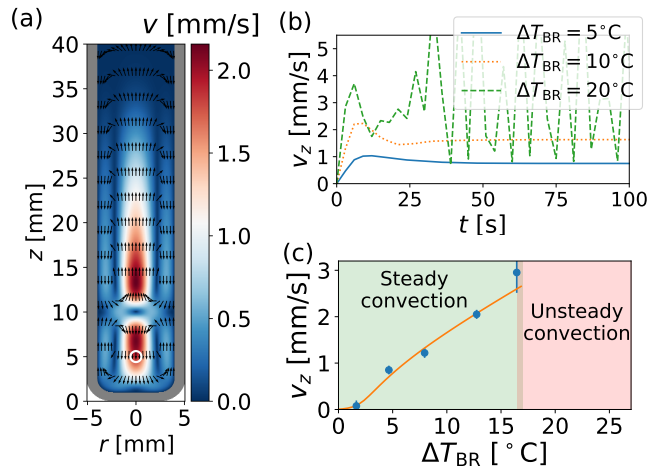


FIG. 3. Predictions obtained by COMSOL simulations. (a) Velocity profile in stationary conditions, for a temperature gradient given by  $\Delta T_{\text{BR}} = 10^\circ\text{C}$ . The white circle denotes the measurement point in our DLS device. (b) Time evolution of  $v_z$  at the measurement point for different temperature gradients. (c)  $v_z$  at the measurement point as a function of the temperature difference,  $\Delta T_{\text{BR}}$  (line). Symbols represent the experimental data, obtained from the average over ten independent HDLS measurements using Eq. (5).

is depicted in Fig. 3(a), with the experimental measurement point highlighted by a circle, inside which magnitudes vary less than 1%, and the drift velocities are completely vertical. The temperature there is lower than bath temperature as an effect of the convection currents. We see two convective regions over and under the bath level.

However, when  $\Delta T_{\text{BR}}$  becomes significantly large, the system dynamics undergo significant alterations. This is evident from Figure 3(b), where the time evolution of vertical velocity at the measuring point for different  $\Delta T_{\text{BR}}$  is presented. For  $\Delta T_{\text{BR}}$  of  $5^\circ\text{C}$  and  $10^\circ\text{C}$ , the system stabilizes between 30 to 40 seconds. However, at  $\Delta T_{\text{BR}} = 20^\circ\text{C}$ , a steady state is unattainable, indicating a transition to a non-stationary regime. This behavior aligns entirely with the experimental observations, which identifies two regimes based on the  $\Delta T_{\text{BR}}$ . In the first regime, for  $\Delta T_{\text{BR}} < 17^\circ\text{C}$ , a roughly linear relationship with velocity exists within a laminar flow regime. This relationship is depicted in Figure 3(c), where experimental and COMSOL simulation results (represented by symbols and a solid line, respectively) closely match, confirming the simulations accuracy in replicating the fluid dynamics. In the second regime, above  $\Delta T_{\text{BR}} = 17^\circ\text{C}$ , the system shifts into an unsteady convective state. Within this regime, the drift velocity displays pronounced temporal fluctuations, (as shown in Fig. 3(b)), in consistency with experimental observations.

A physical explanation of the stationary to non-stationary transition observed in both experiments and fluid dynamics simulations can be explained in terms of the Rayleigh number ( $\text{Ra} = \frac{g\beta\Delta T L^3}{\nu\alpha}$ ), which compares the time scales for thermal transport via diffusion and via convection. According to the literature, there is a critical value,  $\text{Ra}_c$ , at which the

fluid transits from an steady convection state towards a laminar but unsteady convection regime that depends on the geometry [34–37]. Using the experimental values of the height of the measurement cell ( $L = 3.0$  cm), thermal diffusivity of water ( $\alpha = 1.43 \cdot 10^{-7} \text{m}^2/\text{s}$ ), kinematic viscosity ( $\nu = 8 \cdot 10^{-7} \text{m}^2/\text{s}$ ), gravity ( $g = 9.81 \text{m/s}^2$ ), thermal expansion coefficient ( $\beta = 4 \cdot 10^{-4} \text{K}^{-1}$ ) and temperature difference at the transition, we find that  $\text{Ra}_c \approx 1.5 \cdot 10^7$ , which agrees with the value reported in the literature for a similar cell geometry using adiabatic walls [38].

In summary, this study provides nuanced insights into particle dynamics within convection-diffusion systems, extending the conventional use of HDLS. A notable finding is the elucidation of the underlying physical mechanisms driving the oscillatory behavior of the autocorrelation functions, suggesting that these phenomena can occur in a wider range of scenarios than previously assumed. Additionally, our research provides an explanation for the loss of correlation observed in convective systems via HDLS. Our work contributes to a broader application of DLS in studying non-equilibrium states and provides new insights into the temperature-dependent behavior of particles in convection-diffusion scenarios. This research enriches the understanding of particle dynamics in such systems and underscores the continued importance of HDLS as a valuable tool in exploring complex fluid dynamics.

We are grateful to Prof. Antonio M. Puertas-Lopez (University of Almería) and Prof. Alberto Fernández-Nieves for their insightful comments. The authors acknowledge grant PID2022-136540NB-I00 funded by MCIN/AEI/10.13039/501100011033 and ERDF *A way of making Europe*. J.L.M. thanks the Ph.D. student fellowship (FPU21/03568) supported by the Spanish *Ministerio de Universidades*.

---

\* moncho@ugr.es.

† mtorrado@ugr.es.

- [1] F. Yang, L. Xu, and J. Huang, *ES Energy & Environment* **6**, 45 (2019).
- [2] L. Ray, J. J. Iff, and J. J. Heys, *Fluids and Barriers of the CNS* **16**, 1 (2019).
- [3] G. Ibbeken, G. Green, and M. Wilczek, *Physical Review Letters* **123**, 114501 (2019).
- [4] S. Stock, R. von Klitzing, and A. Rahimzadeh, arXiv preprint arXiv:2307.12696 (2023).
- [5] X. Feng, G. Huang, J. Qiu, L. Peng, K. Luo, D. Liu, and P. Han, *Optics Communications* **531**, 129225 (2023).
- [6] J. Lee, W. Wu, J. Y. Jiang, B. Zhu, and D. A. Boas, *Optics express* **20**, 22262 (2012).
- [7] A. Schavkan, *Dynamics of colloidal systems of magnetic nanoparticles under influence of magnetic fields investigated by XPCS*, Ph.D. thesis, Staats-und Universitätsbibliothek Hamburg Carl von Ossietzky (2017).
- [8] J. Wagner, C. Märkert, B. Fischer, and L. Müller, *Physical review letters* **110**, 048301 (2013).
- [9] Y. Chushkin, A. Gulotta, F. Roosen-Runge, A. Pal, A. Stradner, and P. Schurtenberger, *Physical Review Letters* **129**, 238001 (2022).
- [10] T. Thurn-Albrecht, W. Steffen, A. Patkowski, G. Meier, E. W. Fischer, G. Grübel, and D. Abernathy, *Physical Review Letters* **77**, 5437 (1996).
- [11] E. Moulin, I. A. Nyrkova, N. Giuseppone, A. N. Semenov, and E. Buhler, *Soft Matter* **16**, 2971 (2020).
- [12] J. Josefowicz and F. Hallett, *Applied Optics* **14**, 740 (1975).
- [13] A. Sehgal and T. A. Seery, *Macromolecules* **32**, 7807 (1999).
- [14] V. Ruseva, M. Lyons, J. Powell, J. Austin, A. Malm, and J. Corbett, *Colloids and Surfaces A: Physicochemical and Engineering Aspects* **558**, 504 (2018).
- [15] W. Schaertl and C. Roos, *Physical Review E* **60**, 2020 (1999).
- [16] G. Fuller, J. Rallison, R. Schmidt, and L. Leal, *Journal of Fluid Mechanics* **100**, 555 (1980).
- [17] A. B. Leung, K. I. Suh, and R. R. Ansari, *Applied optics* **45**, 2186 (2006).
- [18] O. D. Parashchuk, T. V. Laptinskaya, M. S. Ananieva, and D. Y. Parashchuk, *Soft Matter* **7**, 5585 (2011).
- [19] P. Falus, M. Borthwick, S. Narayanan, A. Sandy, and S. Mochrie, *Physical Review Letters* **97**, 066102 (2006).
- [20] K. Katayama, H. Nomura, H. Ogata, and T. Eitoku, *Physical Chemistry Chemical Physics* **11**, 10494 (2009).
- [21] N. Carl, J. Sindram, M. Gallei, S. U. Egelhaaf, and M. Karg, *Physical Review E* **100**, 052605 (2019).
- [22] R. Pecora, *Dynamic light scattering: applications of photon correlation spectroscopy* (Springer Science & Business Media, 1985).
- [23] J. K. Dhont, *An introduction to dynamics of colloids* (Elsevier, 1996).
- [24] W. I. Goldberg, *American Journal of Physics* **67**, 1152 (1999).
- [25] B. J. Berne and R. Pecora, *Dynamic light scattering: with applications to chemistry, biology, and physics* (Courier Corporation, 2000).
- [26] K. Schätzel, *Journal of modern optics* **38**, 1849 (1991).
- [27] L. B. Aberle, P. Hülstede, S. Wiegand, W. Schröer, and W. Staude, *Applied Optics* **37**, 6511 (1998).
- [28] G. D. Phillies, *The Journal of Chemical Physics* **74**, 260 (1981).
- [29] P. Pusey, *Current opinion in colloid & interface science* **4**, 177 (1999).
- [30] D. Chowdhury, C. M. Sorensen, T. Taylor, J. Merklin, and T. Lester, *Applied optics* **23**, 4149 (1984).
- [31] Y. Sun, G. Carini, M. Chollet, F.-J. Decker, M. Dunne, P. Fuoss, S. O. Hruszkewycz, T. J. Lane, K. Nakahara, S. Nelson, *et al.*, *Physical Review Letters* **127**, 058001 (2021).
- [32] S. Busch, T. H. Jensen, Y. Chushkin, and A. Fluerasu, *The European Physical Journal E* **26**, 55 (2008).
- [33] L. M. Torquato, N. Hélaine, Y. Cui, R. O’Connell, J. Gummel, E. S. Robles, D. Jacob, and J. T. Cabral, *Lab on a Chip* **23**, 2540 (2023).
- [34] S. Chandrasekhar, *Hydrodynamic and hydromagnetic stability* (Courier Corporation, 2013).
- [35] R. Clever and F. Busse, *Journal of Fluid Mechanics* **65**, 625 (1974).
- [36] J. Patterson and J. Imberger, *Journal of Fluid Mechanics* **100**, 65 (1980).
- [37] P. Oresta, G. Stringano, and R. Verzicco, *European Journal of Mechanics-B/Fluids* **26**, 1 (2007).
- [38] P. Le Quére, *Physics of Fluids A: Fluid Dynamics* **2**, 503 (1990).